

Extreme-value modelling of the brightest galaxies at $z \gtrsim 9$

Cameron Heather,¹* Teeraparb Chantavat,² Siri Chongchitnan,¹ and Joseph Silk^{3,4,5}

¹Warwick Mathematics Institute, University of Warwick, Zeeman Building, Coventry CV4 7AL, UK

²Institute for Fundamental Study, Naresuan University, Phitsanulok, 65000, Thailand

³Institut d'Astrophysique de Paris, 98 bis Boulevard Arago, 75014, Paris, France

⁴William H. Miller III Department of Physics and Astronomy, The Johns Hopkins University, Baltimore, MD 21218, USA

⁵BIPAC, Department of Physics, University of Oxford, Keble Road, Oxford OX1 3RH, UK

Accepted XXX. Received YYY; in original form ZZZ

ABSTRACT

Data from the James Webb Space Telescope have revealed an intriguing population of bright galaxies at high redshifts. In this work, we use extreme-value statistics to calculate the distribution (in UV magnitude) of the brightest galaxies in the redshift range $9 \lesssim z \lesssim 16$. We combine the Generalised Extreme Value (GEV) approach with modelling of the galaxy luminosity function. We obtain predictions of the brightest galaxies for a suite of luminosity functions, including the Schechter and double power law functions, as well as a model parametrised by the stellar formation efficiency f_* . We find that the *JWST* data is broadly consistent with f_* of 5% – 10%, and that the brightest galaxy at $z \sim 16$ will have $M_{UV} \approx -23.5_{0.4}^{0.8}$. If f_* is dependent on halo mass, we predict $M_{UV} \approx -22.5_{1.5}^{0.5}$ for such an object. We show that extreme-value statistics not only predicts the magnitude of the brightest galaxies at high redshifts, but may also be able to distinguish between models of star formation in high-redshift galaxies.

Key words: galaxies: luminosity function, mass function – galaxies: star formation – galaxies: statistics – methods: statistical

1 INTRODUCTION

One of the primary objectives of contemporary astronomy and cosmology is to understand the history of our Universe by studying the process of galaxy formation and evolution (Bromm & Yoshida 2011; Stark 2016; Ouchi et al. 2020; Robertson 2022). In pursuit of this goal, the new generation of galaxy surveys are currently underway, particularly at unprecedentedly high redshifts (Gardner et al. 2006; Laureijs et al. 2011; Fomalont et al. 2015; Spergel et al. 2015; DeBoer et al. 2017; Marchetti et al. 2017).

One of the essential ingredients for studying galaxy evolution is the rest-frame ultraviolet (UV) luminosity function (LF), which characterises the density of galaxies within a given volume based on their luminosity. The UV LF is well constrained within the redshift range of $2 \lesssim z \lesssim 10$ based on observations from the *Hubble Space Telescope* (*HST*) and *Spitzer*, predating the launch of the *James Webb Space Telescope* (*JWST*) in 2021. Many studies at that time suggest a rapid decline of the UV LF at the bright end and find that it is well described by the Schechter function (Ellis et al. 2013; Madau & Dickinson 2014; Bouwens et al. 2015, 2021; Finkelstein et al. 2015; Ishigaki et al. 2018; Oesch et al. 2018). However, some evidence suggests that the decline at the bright end of the UV LF is not as steep as predicted by the Schechter function. (Hathi et al. 2012; Finkelstein et al. 2013; Bowler et al. 2014, 2020; McLeod et al. 2024). Some authors have proposed that the bright end of the UV LF at $z \sim 4 - 7$ ($M_{UV} < -24$) cannot be adequately explained by the Schechter function alone, suggesting the necessity for either a

double power law or a modified Schechter function to better account for observational findings (Ono et al. 2018).

The early release of *JWST*/NIRCam data in July 2022 has enabled us to investigate the UV LF at redshifts beyond 10, with the furthest candidate at approximately $z \sim 16$ through photometry (Castellano et al. 2022, 2023; Finkelstein et al. 2022; Naidu et al. 2022; Adams et al. 2023; Atek et al. 2023; Bradley et al. 2023; Labbé et al. 2023; Tacchella et al. 2023a,b), along with some spectroscopic redshift determinations (Schaerer et al. 2022; Arrabal Haro et al. 2023a; Bunker et al. 2023; Curti et al. 2023; Curtis-Lake et al. 2023; Heintz et al. 2023b,a; Harikane et al. 2024). Instead of the rapid decline in UV LF described by the Schechter function at the bright end, recent data from *JWST* indicates a more gradual decrease, better captured by a double power law (Finkelstein et al. 2022; Naidu et al. 2022; Donnan et al. 2023, 2024).

The reasons for the deviation from a Schechter function to a double power law at high redshifts are varied and speculative. Explanations include: a high star formation efficiency at high redshifts (Harikane et al. 2024), the top-heavy nature of the stellar initial mass function for Population III stars (Finkelstein et al. 2023; Bovill et al. 2024; Lapi et al. 2024), the removal of interstellar dust through radiatively driven outflows during the initial stages of galaxy formation (Ferrara et al. 2023; Fiore et al. 2023; Ziparo et al. 2023), short-term variation in dust attenuation (Mirocha & Furlanetto 2023), reduced negative or even positive feedback at early times (Silk et al. 2024), or a combination of these effects.

High-redshift galaxies by the *JWST* are expected to be amongst the most luminous within the field of view at their respective redshifts. Consequently, it is essential to account for any potential biases that

* E-mail: cameron.heather@warwick.ac.uk

may arise when interpreting the UV luminosity function from those luminous galaxies especially at the bright end of the UV LF. In other words, it is crucial to determine whether the UV-bright galaxies observed are representative of the extreme population from the tail end of the luminosity distribution. In this study, we will address this question using *extreme-value statistics* and derive a semi-analytical model of the luminosity distribution for the brightest galaxies at high redshifts and compare that with *JWST* observation.

A pioneering work on using extreme-value statistics to study bright galaxies was [Bhavsar & Barrow \(1985\)](#). They modelled the distribution of the brightest galaxies in groups and clusters at a redshift range $z < 3$ using what is now known as the Generalised Extreme-Value distribution (which we will discuss later in section 3). Our work naturally follows their footsteps but extends the scope to a larger population of galaxies using a more sophisticated modelling of galaxy characteristics.

This paper will be organised as follows: in section 2, we will describe models of the galaxy luminosity function. Alongside the Schechter and the double power law functions, we will introduce the star formation efficiency model, which is parametrised by the star formation efficiency f_* . In section 3, we will introduce a formalism for determining the distribution of the most luminous high-redshift galaxies using extreme-value statistics and compare our theoretical model with the *JWST* data. In section 4, we expand our model by introducing variations in the star formation efficiency with respect to halo mass. Our conclusions and discussion will be presented in section 5.

We will assume a flat Λ CDM cosmology with $H_0 = 68.0 \text{ km s}^{-1} \text{ Mpc}^{-1}$, $\Omega_m = 0.307$, $\Omega_\Lambda = 0.693$, $\Omega_b = 0.046$ and $\sigma_8 = 0.823$.

2 THE LUMINOSITY FUNCTION

The luminosity function gives the number density of galaxies per intrinsic luminosity interval $[L, L + dL]$ at a given redshift. We will use the absolute UV magnitude, M_{UV} , as a measure of luminosity, L , via the relation

$$M_{\text{UV}} - M_{\text{UV}}^* = -2.5 \log_{10} \left(\frac{L}{L^*} \right), \quad (1)$$

where M_{UV}^* is a characteristic magnitude and L^* is a characteristic luminosity which are introduced to allow the functions to be fitted to some observed data.

We now discuss two approaches to obtain the luminosity function of high-redshift galaxies. The first method is to fit the luminosity function to observational data using the double power law and Schechter functions. The second method uses a halo mass function combined with a model of the stellar formation rate.

2.1 Double Power Law and Schechter Models

The double power law function is used to model the luminosity of galaxy groups and clusters ([Holmberg \(1969\)](#), [Tempel et al. \(2009\)](#)) and of radio galaxies and quasars ([Dunlop & Peacock \(1990\)](#)). We take the form of the double power law luminosity function from [Harikane et al. \(2024\)](#):

$$\frac{dn}{dM_{\text{UV}}} = \frac{\ln 10}{2.5} \varphi^* \times \left[10^{0.4(\alpha+1)(M_{\text{UV}} - M_{\text{UV}}^*)} + 10^{0.4(\beta+1)(M_{\text{UV}} - M_{\text{UV}}^*)} \right]^{-1}, \quad (2)$$

where the parameters are given by ([Harikane et al. 2023](#)):

$$\begin{aligned} M_{\text{UV}}^* &= -0.09(z - 9) - 19.33, \\ \log \varphi^* &= -0.28(z - 9) - 3.50, \\ \alpha &= -2.10, \\ \beta &= 0.15(z - 9) - 3.27. \end{aligned}$$

Fig. 1 shows this luminosity function (black solid lines, labelled DPL) plotted against magnitude M_{UV} , along with the other luminosity functions that we will be exploring in this work.

Next, the Schechter model ([Schechter 1976](#)) for the luminosity function is given by

$$\frac{dn}{dL} = \varphi^* \left(\frac{L}{L^*} \right)^\alpha \exp \left(-L/L^* \right), \quad (3)$$

where φ^* and α are the model parameters. Combining this with equation (1), the Schechter luminosity function can be expressed as

$$\frac{dn}{dM_{\text{UV}}} = \frac{\ln 10}{2.5} \varphi^* \left(-10^{0.4(M_{\text{UV}} - M_{\text{UV}}^*)} \right)^{\alpha+1} \times \exp \left[-10^{0.4(M_{\text{UV}} - M_{\text{UV}}^*)} \right], \quad (4)$$

where the parameters are given by ([Harikane et al. 2023](#)):

$$\begin{aligned} M_{\text{UV}}^* &= -0.32(z - 9) - 21.24, \\ \log(\varphi^*) &= -0.08(z - 9) - 4.83, \\ \alpha &= -2.35. \end{aligned}$$

We also plot the Schechter function against magnitude in Fig. 1 (black dashed lines).

2.2 The Star Formation Efficiency Model

In this model, we start by modelling the abundance of bright galaxies using a halo mass function coupled with some model of the stellar formation rate (SFR). A particularly simple model of the SFR (previously used in [Harikane et al. \(2024\)](#)) is given by:

$$\text{SFR} = f_* \times f_b \times \frac{dM_h}{dt} (M_h, z), \quad (5)$$

where f_* is the *star formation efficiency*, $f_b \equiv \Omega_b/\Omega_m$ is the cosmic baryon fraction, and dM_h/dt is the matter accretion rate for a halo of mass M_h . We will use the model of the accretion rate given in [Behroozi & Silk \(2015\)](#).

In this section, we will take f_* to be constant, taking the values 0.02, 0.05, 0.15, 0.4, 1 (section 4 discusses a more sophisticated model of f_*). We then convert the SFR into UV luminosity, L_{UV} , via

$$L_{\text{UV}} (\text{erg s}^{-1} \text{Hz}^{-1}) = \text{SFR} (M_\odot \text{yr}^{-1}) / (1.15 \times 10^{-28}). \quad (6)$$

Combining equations (5) and (6), we obtain an equation for luminosity in terms of halo mass, M_h .

Next, luminosity is converted to UV magnitude using values taken from [Oke & Gunn \(1983\)](#), such that equation (1) becomes

$$M_{\text{UV}} = -2.5 \log_{10} \left(\frac{L_{\text{UV}}}{\text{erg s}^{-1} \text{Hz}^{-1}} \right) + 51.6. \quad (7)$$

This gives us the following relation between the UV magnitude and halo mass.

$$M_{\text{UV}} (M_h, z) = -2.5 \log_{10} (\dot{M}_h) - 2.5 \log_{10} \left(\frac{f_* \times f_b}{1.15 \times 10^{-28}} \right) + 51.6 \quad (8)$$

Taking the derivative with respect to M_h , we obtain

$$\frac{dM_{UV}}{dM_h} = -\frac{2.5}{\ln(10)} \frac{\ddot{M}_h}{\dot{M}_h^2}. \quad (9)$$

We now introduce the halo mass function, dn/dM_h , defined as the number of dark matter haloes per unit mass interval $[M_h, M_h + dM_h]$.

$$\frac{dn}{dM_h} = f(\sigma) \frac{\bar{\rho}_m}{M_h} \frac{d \ln \sigma^{-1}}{dM_h}. \quad (10)$$

In this work, we will use the Tinker mass function (Tinker et al. 2008) in which

$$f(\sigma) = A \left[\left(\frac{\sigma}{b} \right)^{-a} + 1 \right] e^{-c/\sigma^2}, \quad (11)$$

where σ is the variance of the smoothed linear density field, and the parameters A , b and c depend on redshift. The luminosity function can then be expressed via the chain rule as:

$$\frac{dn}{dM_{UV}} = \frac{dn}{dM_h} \left| \frac{dM_h}{dM_{UV}} \right| \quad (12)$$

$$= \frac{dn}{dM_h} \times 0.4 \ln(10) \left| \frac{\dot{M}_h^2}{\ddot{M}_h} \right|. \quad (13)$$

In equation (13), there appears to be no direct dependence on f_* . However, the f_* dependence does arise through the conversion formulae in equations (6) and (8).

We plot the various luminosity functions calculated in this section at four redshifts ($z = 9, 10, 12, 16$) in Fig. 1, where f_* is varied between 0.02 and 1 (the curves for the f_* model are normalised to match those of Harikane et al. (2024)). We see that the Schechter luminosity function is comparable to the f_* model with f_* roughly between 0.02 and 0.05. On the other hand, the double power law function is flatter and predicts a higher number of brighter galaxies than the other models.

3 EXTREME-VALUE MODELLING OF THE BRIGHTEST GALAXIES

Our goal is to obtain a statistical description of the most extreme luminosities of high-redshift galaxies. We will do this using extreme-value statistics, which has previously been used in astrophysics to find the brightest galaxies in clusters by Bhavsar & Barrow (1985), quantify the abundances of the most massive Pop III stars (Chantavat et al. (2023)), predict the most massive galaxy clusters (Davis et al. 2011; Waizmann et al. 2012; Chongchitnan & Silk 2012) and estimate the abundances of extreme primordial black holes and extreme-spin primordial black holes (Chongchitnan et al. 2021; Chongchitnan & Silk 2021).

In particular, we will be working with the generalised extreme-value (GEV) approach, also known as the block maxima method (Gumbel (1958)). In this method, we divide the galaxy population in a given redshift bin into N distinct blocks, from which we identify the brightest galaxy in each block using a probability density function outlined below. Analogous to the Central Limit Theorem, these brightest galaxies will have a large- N limit distribution corresponding to one of the GEV distributions (equation (18)).

We summarise the GEV pipeline here (more details can be found in White (1979); Davis et al. (2011)). First, we calculate the number density $n(< M_{UV})$ of galaxies with UV magnitude less than M_{UV} as

$$n(< M_{UV}, z) = \int_{-\infty}^{M_{UV}} \frac{dn}{dM'_{UV}} dM'_{UV}. \quad (14)$$

Note that, by the definition of M_{UV} , equation (14) counts the *brightest* galaxies. The redshift dependence can then be integrated out to obtain the number count of the brightest galaxies in the redshift interval $[z_0, z_1]$:

$$n(< M_{UV}) = \int_{z_0}^{z_1} n(< M_{UV}, z) dz. \quad (15)$$

Next, to predict the brightest magnitude that galaxies could have at high redshifts, we consider the probability that no galaxies in a given volume V exceed this extreme brightness. This probability can be modelled as the Poisson distribution with the following cumulative distribution function (cdf):

$$P_0(M_{UV}) = \exp(-n(< M_{UV})V), \quad (16)$$

Differentiating this with respect to M_{UV} , we obtain the probability density function (pdf):

$$\frac{dP_0}{dM_{UV}} = -V \frac{dn(< M_{UV})}{dM_{UV}} \exp(-n(< M_{UV})V), \quad (17)$$

The Fisher-Tippett-Gnedenko theorem implies that in the large- N limit, the cdf (equation (16)) approaches the GEV distribution given by:

$$G(M_{UV}) = \begin{cases} \exp[-(1 + \gamma y)^{-1/\gamma}] & (\gamma \neq 0), \\ \exp[-e^{-y}] & (\gamma = 0), \end{cases} \quad (18)$$

where $y := (M_{UV} - \alpha)/\beta$, with α describing the location of the peak, and β describing the scale of the pdf. The sign of the parameter γ determines the GEV type, with $\gamma = 0$, $\gamma > 0$ and $\gamma < 0$, corresponding to the Gumbel, Fréchet and Weibull distributions respectively.

We can express the GEV parameter α, β, γ in terms of astrophysical parameters by Taylor-expanding the Poisson distribution $P_0(M_{UV})$ and the GEV distribution $G(M_{UV})$ around the peak of the pdf at M_{peak} to cubic order. By equating the coefficients, we find

$$\begin{aligned} \gamma &= n(< M_{\text{peak}})V - 1, \\ \beta &= \frac{(1 + \gamma)^{1+\gamma}}{\left. \frac{dn}{dM_{UV}} \right|_{M_{\text{peak}}}} V, \\ \alpha &= M_{\text{peak}} - \frac{\beta}{\gamma} \left((1 + \gamma)^{-\gamma} - 1 \right), \end{aligned} \quad (19)$$

While these equations provide a good approximation to the values γ , α and β , using a numerical approximation produces a closer fit to the Poisson pdf (equation (17)), which we use to plot the GEV distribution in Fig. 2. This method assumes the pdfs are well described by the Gumbel distribution, taking $\gamma \approx 0$.

3.1 Extreme-value pdf of the brightest galaxies

We plot the pdf for the distribution of the brightest galaxies in Fig. 2 for 4 redshift bins: $z \in [9, 10]$, $[10, 11]$, $[12, 13]$ and $[16, 17]$. The solid lines are pdfs calculated using equation (17), whilst the dashed lines are the numerical fits assuming that the pdfs are Gumbel type ($\gamma = 0$ in equation (18)). The parameters α and β for the Gumbel fit are given in Table A1. Note that in each bin, α is very close to the magnitude of M_{UV} where the peak of the pdf occurs.

From Fig. 2, we see that at higher redshifts, the pdfs shift to higher values of M_{UV} (meaning that the extreme galaxies are less bright). We also observe that increasing f_* produces brighter extreme galaxies. In particular, increasing f_* from 0.02 to 0.15 results in a pdf peak shift of $\Delta M_{UV} \approx -2$.

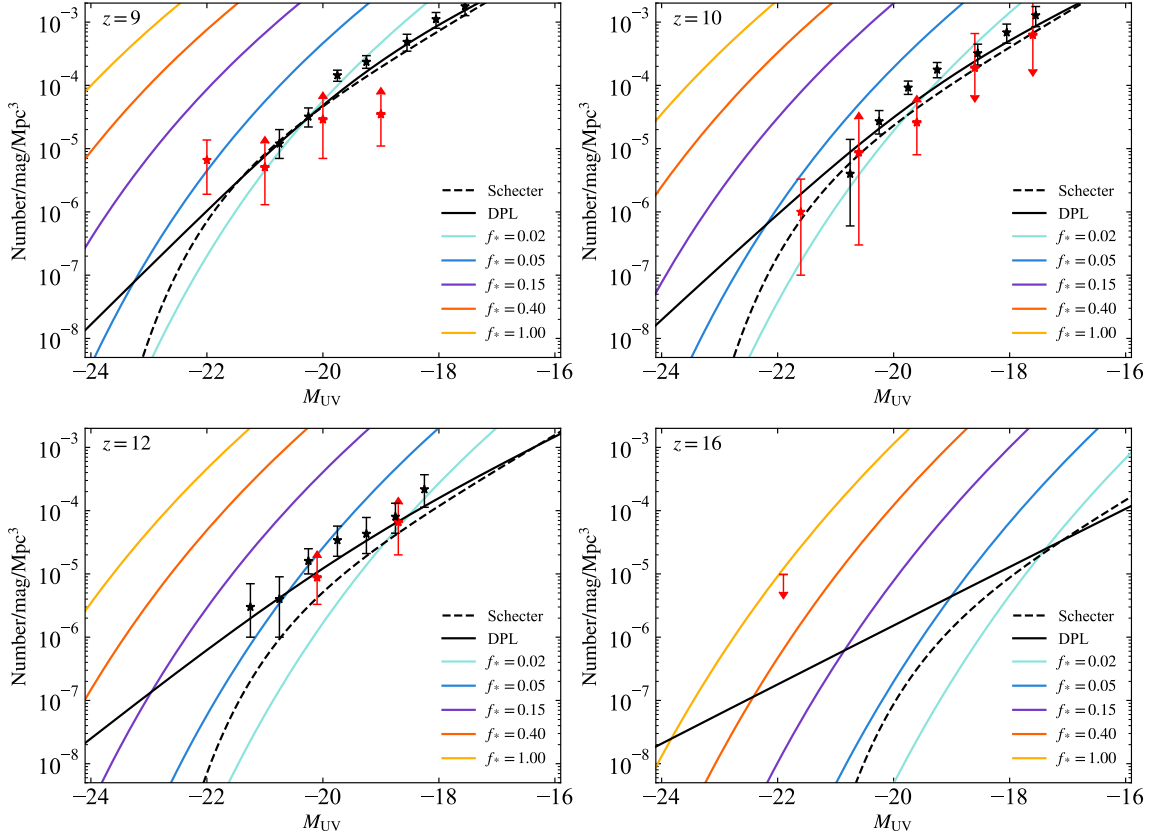


Figure 1. Comparison of the luminosity functions dn/dM_{UV} at $z = 9$ (upper-left), $z = 10$ (upper-right), $z = 12$ (lower-left) and $z = 16$ (lower-right). The black solid and dashed curves are the double power law and Schechter luminosity functions respectively, calculated in section 2.1. The colourful curves correspond to the f_* model of the luminosity function in section 2.2 (see equation (13)). The colourful curves correspond to $f_* = 0.02, 0.05, 0.15, 0.4, 1$, with amplitudes matching those of Harikane et al. (2024). The red data points correspond to spectroscopic data from Harikane et al. (2024), and the black points correspond to photometric data from Donnan et al. (2024).

3.2 Comparison with *JWST* data

We now study the redshift dependence of the extreme-value predictions more closely. In Fig. 3 and 4, we plot the peak of the Gumbel pdf for the brightest galaxies over the redshift range $z = 9 - 16$ (dashed lines). We also indicate the 95th and 99th percentiles of the pdfs (shaded dark and light colours). Fig. 3 shows the extreme-value predictions for M_{UV} for the double power law and Schechter models. Fig. 4 shows the same predictions for the f_* model with $f_* = 0.02, 0.05$ and 0.15 .

On these plots, we have included data from the *JWST* Early Release Science programs CEERS and GLASS. In particular, we have selected the brightest galaxies from a collection of recent studies on these galaxies (Donnan et al. (2023), Bowler et al. (2020), Harikane et al. (2022b), Harikane et al. (2023), Naidu et al. (2022), Bradley et al. (2023), Arrabal Haro et al. (2023a), Arrabal Haro et al. (2023b), Tacchella et al. (2023b), Harikane et al. (2024)). Most of these studies obtained the photometric redshifts for the galaxies using the EAZY or PROSPECTOR pipeline. While the redshifts have not been spectroscopically confirmed, the papers have published redshift uncertain-

ties, which we have displayed as error bars. We also include spectroscopically confirmed galaxies from Arrabal Haro et al. (2023a), Arrabal Haro et al. (2023b), Tacchella et al. (2023b), Harikane et al. (2024).

3.2.1 Double power law and Schechter models

In Fig. 3, we note that neither the double power law or Schechter model produces a satisfactory prediction for the peak magnitudes of the brightest galaxies. We discuss these separately below.

The double power law model (left panel) gives an unphysical prediction that the most luminous galaxies are *brighter* at higher redshifts. We note that the unphysical trend can be corrected by an ad-hoc change in the sign dB/dz in equation (2). We will revisit this point in the discussion section.

However, the model overestimates the brightness of extreme galaxies. For example, for $z > 14.5$, the model predicts extreme brightness of $M_{UV} \lesssim -30$. Nevertheless, in principle, the model is consistent with observation as long as the data points are above the peak-brightness band.

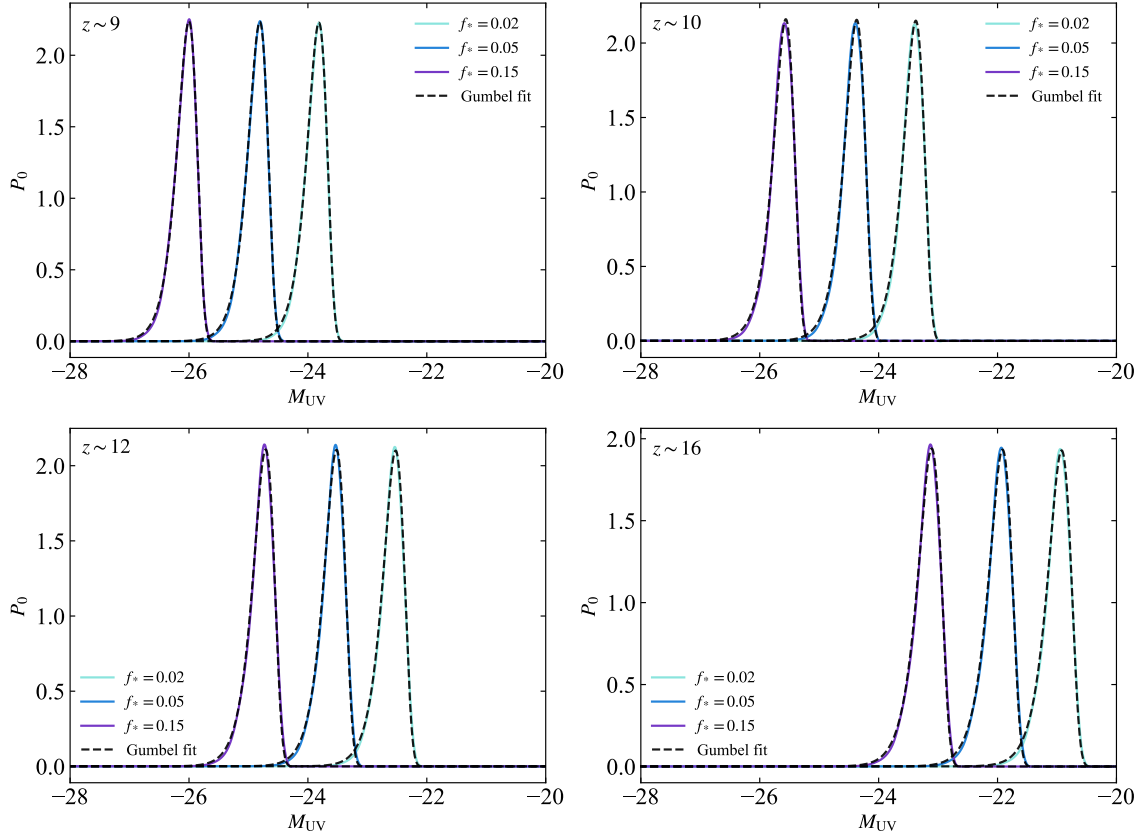


Figure 2. The probability density functions for the most luminous galaxies calculated in section 2.2 for 4 redshift bins: $z = [9, 10]$ (upper-left), $[10, 11]$ (upper-right), $[12, 13]$ (lower-left) and $[16, 17]$ (lower-right). The solid coloured lines are the pdfs derived from the Poisson distribution (equation (17)), assuming 3 values for the star formation efficiency: $f_* = 0.02$ (cyan), 0.05 (blue) and 0.15 (purple). The dashed lines are the Gumbel distribution (equation (18)) with parameters α, β given in Table A1.

Next, using the Schechter model (right panel), we find that the width of the pdf is much smaller. As a result, the coloured band barely contains any of the the extreme data points, and, more worryingly, we also see observed galaxies that are brighter than the predicted extreme brightness.

3.2.2 The f_* model

In Fig. 4 three of the star formation efficiency models have been plotted, $f_* = 0.02, 0.05, 0.15$. The model with $f_* = 0.02$ is comparable to the Schechter model discussed above. The model with $f_* = 0.05$ (blue band) appears to be consistent with the data points, with the implication that these galaxies are expected to be the brightest we would observe. The model with $f_* = 0.15$ is also consistent with the data, in the sense that all the data points correspond to galaxies that are less bright than the extreme-value prediction.

The extreme-value modelling allows us to extrapolate to higher redshifts. For example, assuming $f_* = 0.15$, at $z \sim 16$ we expect to see galaxies no brighter than $M_{UV} \sim -23.5_{0.4}^{0.8}$. Future observations can be added to such a plot, giving us additional constraints on the star formation efficiency f_* .

4 EXTENDING THE f_* MODEL

A natural extension to the f_* model is to consider the case when the star formation efficiency is not a constant. Our goal is to obtain the extreme-value pdf for the brightest galaxies in this model.

One such model is that of Tacchella et al. (2018) in which f_* has a dependence on the halo mass M_h in the form of the double power law function:

$$f_* = \frac{\text{SFR}}{\dot{M}_h} = 2\epsilon_0 \left[\left(\frac{M_h}{M_c} \right)^{-\mu} + \left(\frac{M_h}{M_c} \right)^{\nu} \right]^{-1}, \quad (20)$$

where ϵ_0 is a normalisation constant, M_c is a characteristic mass where the efficiency is equal to ϵ_0 , and μ and ν are slopes that determine the behaviour at high and low masses. This equation has been calibrated at $z = 4$, with parameter values:

$$\text{Tacchella model: } (\epsilon_0, M_c, \mu, \nu) = (0.22, 6.3 \times 10^{10} M_\odot, 0.89, 0.4). \quad (21)$$

We also see the same form in Harikane et al. (2022a) with parameter values:

$$\text{Harikane model: } (\epsilon_0, M_c, \mu, \nu) = (3.2 \times 10^{-2}, 10^{11.5} M_\odot, 1.2, 0.5). \quad (22)$$

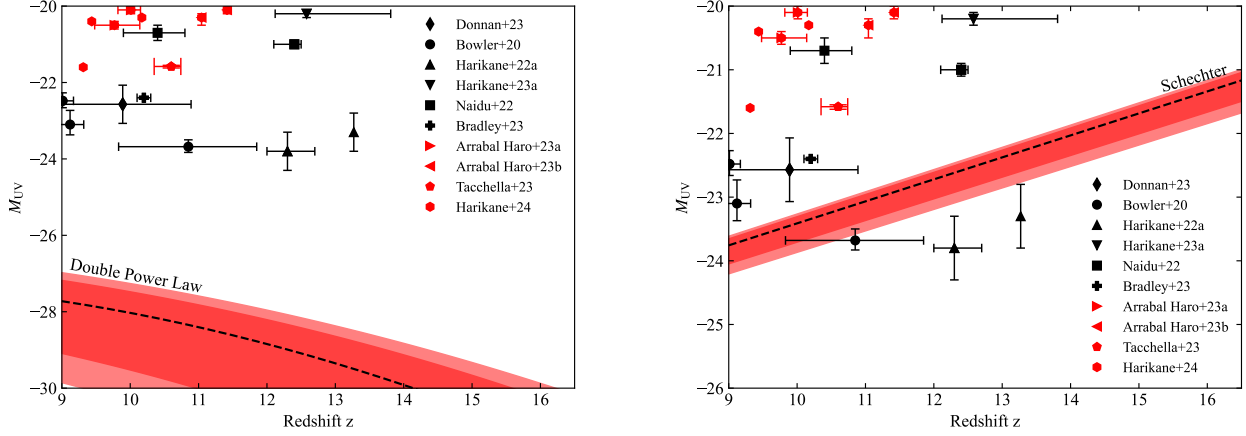


Figure 3. The peak magnitudes M_{peak} (dashed lines) of the extreme-value (Gumbel) pdf for M_{UV} plotted as a function of redshift, assuming the double power law luminosity function from equation (2) (left) and the Schechter luminosity function from equation (4) (right). The darker/lighter regions correspond to the 95th and 99th percentiles of the pdf. The data points are based off the most extreme samples from previous studies (Donnan et al. (2023), Bowler et al. (2020), Harikane et al. (2022b), Harikane et al. (2023), Naidu et al. (2022), Bradley et al. (2023), Arrabal Haro et al. (2023a), Arrabal Haro et al. (2023b), Tacchella et al. (2023b), Harikane et al. (2024)).

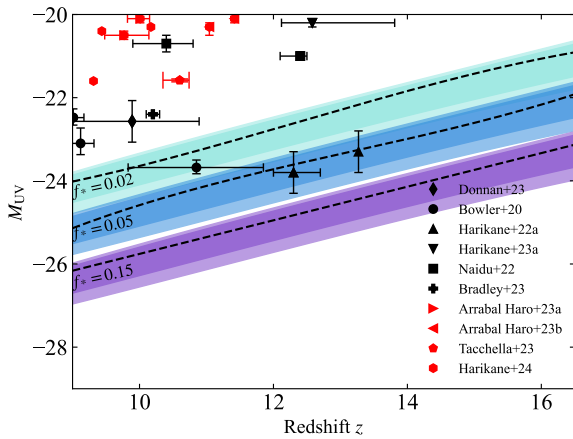


Figure 4. Extreme-value pdf profile (same as Fig. 3) plotted as a function of redshift, for the f_* model with $f_* = 0.02$ (cyan), 0.05 (blue) and 0.15 (purple).

These two models of f_* are plotted in Fig. 5.

We can follow the same method as section 2.2 to find the luminosity function for this mass-dependent f_* , by substituting equation (20) into the working. In particular, our equation for $M_{\text{UV}}(M_h, z)$ (equation (8)) is now

$$M_{\text{UV}}(M_h, z) = -2.5 \log_{10}(\dot{M}_h) + 2.5 \log_{10}(M_*^{-\mu} + M_*^{\nu}) - 2.5 \log_{10}\left(\frac{2\epsilon_0}{K_{\text{UV}}}\right) + 51.6, \quad (23)$$

where $M_* = M_h/M_c$. We can then take the derivative with respect to M_h and obtain the luminosity function:

$$\frac{dn}{dM_{\text{UV}}} = \frac{dn}{dM_h} \times 0.4 \ln(10) \left[\frac{\ddot{M}_h}{\dot{M}_h^2} + \frac{\mu M_*^{-\mu} - \nu M_*^{\nu}}{M_h (M_*^{-\mu} + M_*^{\nu})} \right]^{-1}. \quad (24)$$

From this, we introduce the extreme-value methodology from sec-

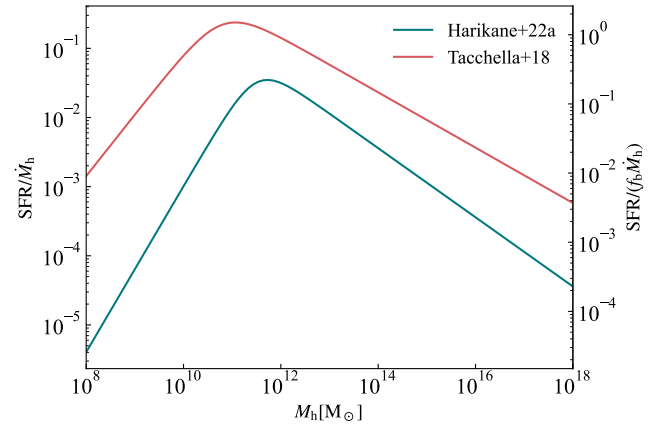


Figure 5. Comparison of two stellar efficiency functions f_* as a function of halo mass M_h . The double-power law form is given in equation (20), with parameter values in equations (21) and (22) for the Tacchella and Harikane models respectively.

tion 3, where we find the peak magnitude for each redshift bin, which we then model using a GEV distribution. We plot the peak of Gumbel pdf, with the 95th and 99th percentile bands, varied over our redshift range, in Fig. 6.

The main difference between Fig. 4 and 6 is the upward curvature of the bands at high redshifts. We also see that the Tacchella model gives a similar extreme-value prediction to the $f_* = 0.15$ model. At $z \sim 16$, the Tacchella curve predicts an extreme brightness of $M_{\text{UV}} = -22.5^{+0.5}_{-1.5}$, which is less bright than what the $f_* = 0.15$ model predicts. The confidence interval in the Tacchella model is also wider at the high- z end of the graph.

The Harikane model, on the other hand, predicts a more conservative set of extreme brightnesses, with some observed bright galaxies barely grazing the 99th percentile band. Around $z \sim 10$, the extreme-value predictions in the Harikane model is comparable to that with constant f_* model with f_* of a few percent. However, the band curves

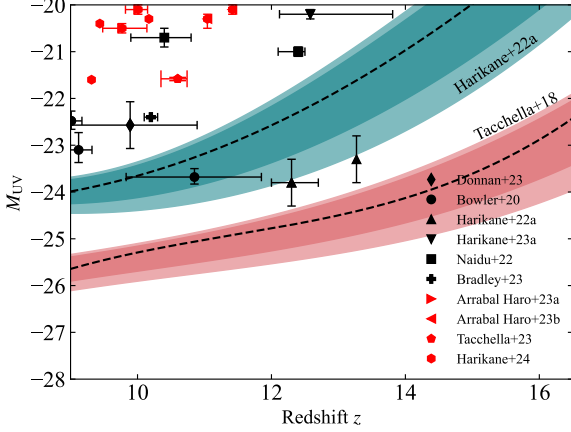


Figure 6. Extreme-value pdf profile (same as Fig. 3) plotted as a function of redshift, for the halo mass-dependent f_* model (equation (20)). The teal (upper) band corresponds to the Harikane model (equation (22)) whilst the pink (lower) band is the Tacchella model (equation (21)).

up rapidly towards higher redshifts. Finally, like the Tacchella model, the band is also much wider than the constant f_* model.

We conclude that both the Tacchella and the Harikane models are consistent with *JWST* observations.

5 CONCLUSION AND DISCUSSION

We have applied extreme-value statistics to predict how bright the most luminous galaxies at high redshifts could be. In particular, we derived the probability distribution (in the UV magnitude M_{UV}) of the brightest galaxies at redshifts $z \sim 9 - 16$. We found that such a distribution is well approximated by the Gumbel distribution. We studied a number of models of the galaxy luminosity function and derived the corresponding extreme-value distributions as a function of redshift. Our main results are shown in Fig. 4 and 6, in which our theoretical results are compared with data from the *JWST*.

Further summary and discussion points are given below.

- *The Generalised Extreme-Value (GEV) formalism* (equation (18)) was used to calculate pdf of the brightest galaxies. We find that the GEV parameter γ (see Table A1) is so small that the extreme-value pdf for M_{UV} is well approximated by the Gumbel distribution, as shown in Fig. 2. The pdf profile (along with the 95th and 99th percentiles) are shown in Fig. 3, 4 and 6, assuming different galaxy luminosity functions as shown in Fig. 1.

- *The Schechter model* of the luminosity function has previously been used to model the luminosity of galaxies at $z \sim 5$. The parameters used in this work (equation (3)) were calibrated using observations at $z \sim 9$. We found that the resulting extreme-value pdf (right panel in Fig. 3) appears to be in tension with the brightest *JWST* galaxies at $z \gtrsim 10$.

- *The double power law model* (equation (2)), on the other hand, resulted in an unphysical extreme-value prediction (left panel in Fig. 3), where extreme galaxies appear brighter at higher redshifts. This might be due to the limited accuracy of the parametrisation (equation (2)). Indeed, we found an ad-hoc correction by switching the sign of $d\beta/dz$ to negative.

Donnan et al. (2024) gave new constraints on the redshift evolution

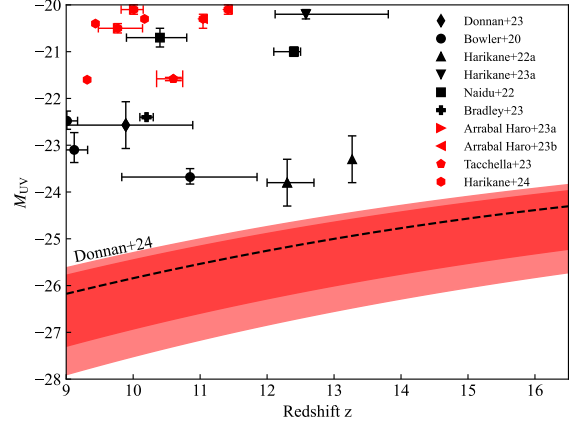


Figure 7. Extreme-value pdf profile (same as Fig. 3) plotted as a function of redshift, for the double power law luminosity function with parameters given in Donnan et al. (2024).

of the double power law luminosity function. We use their data in place of the parametrisation (equation (2)), and obtained the extreme-value pdf profile shown in Fig. 7, which appears to be consistent with data. We note that in their work, $d\beta/dz$ is indeed negative. We conclude that a physical double power law parametrisation must satisfy the condition $d\beta/dz < 0$.

- *The f_* model* of the luminosity function (as outlined in Harikane et al. (2024)) was considered as an alternative to the Schechter and DPL models. This model requires the stellar formation rate f_* , which we initially assumed to be constant, and a halo mass function (taken to be the Tinker mass function). Fig. 4 shows that for constant formation rate, $f_* = 0.02$ produces similar result to that of the Schechter model, whilst f_* between 0.05 and 0.15 produces an extreme-value pdf that is consistent with *JWST* data.

The model predicts that at $z \sim 16$, the brightest galaxies will have a UV magnitude around -23 . Such a prediction depends on the choice of the halo mass function, which may be rapidly evolving at high redshifts Donnan et al. (2024). The Tinker mass function is known predict the halo number density accurately at low redshifts ($z \sim 1-2$) and a recalibration to high- z simulations is needed to confirm if the parameter values remain accurate for $z \sim 9 - 16$.

- *Extending the f_* model* to include a dependence on the halo mass was studied in section 4. In particular, we considered the models of Tacchella et al. (2023b) (equation (21)) and Harikane et al. (2022a) (equation (22)). The extreme-value predictions are shown in Fig. 6, which shows an upward curvature of the bands at high redshifts. The Tacchella model gives a similar result to the constant $f_* = 0.15$ model, whilst the Harikane model is comparable to f_* of a few percent, with the predictions diverging at $z \sim 16$. As more high redshift galaxies are observed, the extreme-value formalism will allow us to distinguish whether f_* is constant or halo mass-dependent.

Fig. 8 summarises the main results of this work: each solid line shows the peak of the extreme-value pdf as a function of redshift, assuming the double power law, constant f_* and variable f_* models that are consistent with *JWST* observation of the brightest high-redshift galaxies.

- *Uncertainties in the data.* We have taken into account neither the

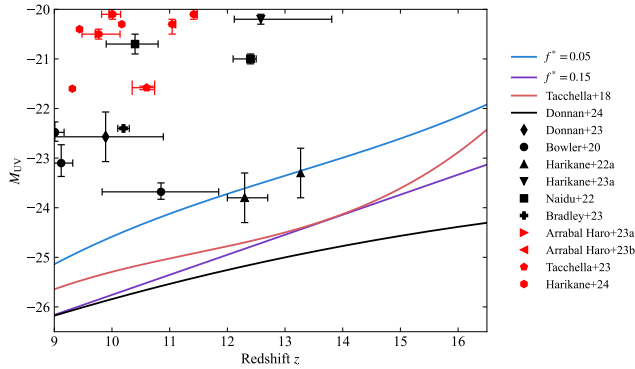


Figure 8. A comparison of various EVS models in this work that are consistent with *JWST* data. Each solid lines shows the peak of the Gumbel distribution (percentile bands not shown). The models for the luminosity function dn/dM_{UV} are: constant f_* (equation (13)), variable f_* (equation (24)), and the double-power law model (equation (2)) assuming the parameters of Donnan et al. (2024).

effects of cosmic variance (in the sense of the statistical uncertainty in observation of rare objects at high redshifts) nor Eddington bias (Trenti & Stiavelli (2008), Teerikorpi (2015)). Both of these could reduce the deduced brightness of extreme galaxies. We leave the calculation of statistical bias to a future work.

ACKNOWLEDGEMENTS

For the purpose of open access, the author has applied a Creative Commons Attribution (CC BY) licence to any Author Accepted Manuscript version arising from this submission. We would like to thank Suraphong Yuma for his useful suggestions.

DATA AVAILABILITY

The data used in this article will be shared on reasonable request to the corresponding author.

REFERENCES

Adams N. J., et al., 2023, *MNRAS*, **518**, 4755
 Arrabal Haro P., et al., 2023a, *Nature*, **622**, 707
 Arrabal Haro P., et al., 2023b, *ApJ*, **951**, L22
 Atek H., et al., 2023, *MNRAS*, **519**, 1201
 Behroozi P. S., Silk J., 2015, *ApJ*, **799**, 32
 Bhavsar S. P., Barrow J. D., 1985, *MNRAS*, **213**, 857
 Bouwens R. J., et al., 2015, *ApJ*, **803**, 34
 Bouwens R. J., et al., 2021, *AJ*, **162**, 47
 Bovill M. S., Stiavelli M., Wiggins A. I., Ricotti M., Trenti M., 2024, *ApJ*, **962**, 49
 Bowler R. A. A., et al., 2014, *MNRAS*, **440**, 2810
 Bowler R. A. A., Jarvis M. J., Dunlop J. S., McLure R. J., McLeod D. J., Adams N. J., Milvang-Jensen B., McCracken H. J., 2020, *MNRAS*, **493**, 2059
 Bradley L. D., et al., 2023, *ApJ*, **955**, 13
 Bromm V., Yoshida N., 2011, *ARA&A*, **49**, 373
 Bunker A. J., et al., 2023, *A&A*, **677**, A88
 Castellano M., et al., 2022, *ApJ*, **938**, L15
 Castellano M., et al., 2023, *ApJ*, **948**, L14
 Chantavat T., Chongchitnan S., Silk J., 2023, *MNRAS*, **522**, 3256
 Chongchitnan S., Silk J., 2012, *Phys. Rev. D*, **85**, 063508

Chongchitnan S., Silk J., 2021, *Phys. Rev. D*, **104**, 083018
 Chongchitnan S., Chantavat T., Zunder J., 2021, *Astronomische Nachrichten*, **342**, 648
 Curti M., et al., 2023, *MNRAS*, **518**, 425
 Curtis-Lake E., et al., 2023, *Nature Astronomy*, **7**, 622
 Davis O., Devriendt J., Colombi S., Silk J., Pichon C., 2011, *MNRAS*, **413**, 2087
 DeBoer D. R., et al., 2017, *PASP*, **129**, 045001
 Donnan C. T., et al., 2023, *MNRAS*, **518**, 6011
 Donnan C. T., et al., 2024, *arXiv e-prints*, p. arXiv:2403.03171
 Dunlop J. S., Peacock J. A., 1990, *MNRAS*, **247**, 19
 Ellis R. S., et al., 2013, *ApJ*, **763**, L7
 Ferrara A., Pallottini A., Dayal P., 2023, *MNRAS*, **522**, 3986
 Finkelstein S. L., et al., 2013, *Nature*, **502**, 524
 Finkelstein S. L., et al., 2015, *ApJ*, **810**, 71
 Finkelstein S. L., et al., 2022, *ApJ*, **940**, L55
 Finkelstein S. L., et al., 2023, *ApJ*, **946**, L13
 Fiore F., Ferrara A., Bischetti M., Feruglio C., Travascio A., 2023, *ApJ*, **943**, L27
 Fomalont E. B., et al., 2015, *ApJ*, **808**, L1
 Gardner J. P., et al., 2006, *Space Sci. Rev.*, **123**, 485
 Gumbel E. J., 1958, *Statistics of extremes*. Columbia university press
 Harikane Y., et al., 2022a, *ApJS*, **259**, 20
 Harikane Y., et al., 2022b, *ApJ*, **929**, 1
 Harikane Y., et al., 2023, *ApJS*, **265**, 5
 Harikane Y., Nakajima K., Ouchi M., Umeda H., Isobe Y., Ono Y., Xu Y., Zhang Y., 2024, *ApJ*, **960**, 56
 Hathi N. P., Mobasher B., Capak P., Wang W.-H., Ferguson H. C., 2012, *ApJ*, **757**, 43
 Heintz K. E., et al., 2023a, *Nature Astronomy*, **7**, 1517
 Heintz K. E., et al., 2023b, *ApJ*, **944**, L30
 Holmberg E., 1969, *Arkiv för Astronomi*, **5**, 305
 Ishigaki M., Kawamata R., Ouchi M., Oguri M., Shimasaku K., Ono Y., 2018, *ApJ*, **854**, 73
 Labbé I., et al., 2023, *Nature*, **616**, 266
 Lapi A., et al., 2024, *arXiv e-prints*, p. arXiv:2403.07401
 Laureijs R., et al., 2011, *arXiv e-prints*, p. arXiv:1110.3193
 Madau P., Dickinson M., 2014, *ARA&A*, **52**, 415
 Marchetti L., Serjeant S., Vaccari M., 2017, *MNRAS*, **470**, 5007
 McLeod D. J., et al., 2024, *MNRAS*, **527**, 5004
 Mirocha J., Furlanetto S. R., 2023, *MNRAS*, **519**, 843
 Naidu R. P., et al., 2022, *ApJ*, **940**, L14
 Oesch P. A., Bouwens R. J., Illingworth G. D., Labbé I., Stefanon M., 2018, *ApJ*, **855**, 105
 Oke J. B., Gunn J. E., 1983, *ApJ*, **266**, 713
 Ono Y., et al., 2018, *PASJ*, **70**, S10
 Ouchi M., Ono Y., Shibuya T., 2020, *ARA&A*, **58**, 617
 Robertson B. E., 2022, *ARA&A*, **60**, 121
 Schaerer D., Marques-Chaves R., Barrufet L., Oesch P., Izotov Y. I., Naidu R., Guseva N. G., Brammer G., 2022, *A&A*, **665**, L4
 Schechter P., 1976, *ApJ*, **203**, 297
 Silk J., Begelman M. C., Norman C., Nusser A., Wyse R. F. G., 2024, *ApJ*, **961**, L39
 Spergel D., et al., 2015, *arXiv e-prints*, p. arXiv:1503.03757
 Stark D. P., 2016, *ARA&A*, **54**, 761
 Tacchella S., Bose S., Conroy C., Eisenstein D. J., Johnson B. D., 2018, *ApJ*, **868**, 92
 Tacchella S., et al., 2023a, *MNRAS*, **522**, 6236
 Tacchella S., et al., 2023b, *ApJ*, **952**, 74
 Teerikorpi P., 2015, *A&A*, **576**, A75
 Tempel E., Einasto J., Einasto M., Saar E., Tago E., 2009, *A&A*, **495**, 37
 Tinker J., Kravtsov A. V., Klypin A., Abazajian K., Warren M., Yepes G., Gottlöber S., Holz D. E., 2008, *ApJ*, **688**, 709
 Trenti M., Stiavelli M., 2008, *ApJ*, **676**, 767
 Waizmann J. C., Etori S., Moscardini L., 2012, *MNRAS*, **420**, 1754
 White S. D. M., 1979, *MNRAS*, **186**, 145
 Ziparo F., Ferrara A., Sommovigo L., Kohandel M., 2023, *MNRAS*, **520**, 2445

APPENDIX A:

Table A1 shows the GEV parameters (α and β) and peak magnitudes for each luminosity function at various redshifts (see equation (18)). The parameters have been calculated numerically using least-square fitting, assuming $\gamma = 0$ (*i.e.* assume that the GEV distribution is the Gumbel type). Alternatively, one can use equation (19) to approximate these values.

This paper has been typeset from a $\text{\TeX}/\text{\LaTeX}$ file prepared by the author.

Luminosity function	Redshift	Peak M_{UV}	α	β
DPL (equation (2))	$z \sim 9$	-27.88	27.86	0.4960
	$z \sim 10$	-28.27	28.21	0.5211
	$z \sim 12$	-29.06	29.09	0.6093
	$z \sim 16$	-31.56	31.58	0.9298
DPL (Donnan et al. 2024)	$z \sim 9$	-26.01	26.02	0.3679
	$z \sim 10$	-25.69	25.69	0.3578
	$z \sim 12$	-25.13	25.14	0.3392
	$z \sim 16$	-24.30	24.31	0.3075
Schechter (equation (4))	$z \sim 9$	-23.59	23.59	0.09729
	$z \sim 10$	-23.25	23.24	0.09917
	$z \sim 12$	-22.56	22.55	0.1030
	$z \sim 16$	-21.17	21.12	0.1112
$f_* = 0.02$ (equation (13))	$z \sim 9$	-23.84	23.82	0.1651
	$z \sim 10$	-23.43	23.38	0.1711
	$z \sim 12$	-22.53	22.52	0.1751
	$z \sim 16$	-20.91	20.92	0.1907
$f_* = 0.05$	$z \sim 9$	-24.85	24.81	0.1647
	$z \sim 10$	-24.34	24.37	0.1706
	$z \sim 12$	-23.54	23.52	0.1747
	$z \sim 16$	-21.92	21.92	0.1902
$f_* = 0.15$	$z \sim 9$	-25.96	26.00	0.1644
	$z \sim 10$	-25.56	25.56	0.1703
	$z \sim 12$	-24.75	24.71	0.1745
	$z \sim 16$	-23.13	23.11	0.1895
$f_*(M_h)$ Tacchella (equation (21))	$z \sim 9$	-25.45	25.42	0.1277
	$z \sim 10$	-25.15	25.18	0.1379
	$z \sim 12$	-24.65	24.59	0.1835
	$z \sim 16$	-22.42	22.41	0.3374
$f_*(M_h)$ Harikane (equation (22))	$z \sim 9$	-23.84	23.77	0.1451
	$z \sim 10$	-23.43	23.40	0.1981
	$z \sim 12$	-22.22	22.11	0.3296
	$z \sim 16$	-18.26	18.20	0.4495

Table A1. The peak magnitude M_{UV} , and the Gumbel parameters α and β for the luminosity functions considered in this paper. The notation $z \sim 9, 10, 12, 16$ refers to the redshift bins [9, 10], [10, 11], [12, 13] and [16, 17] respectively.